Original Article

2D and 3D Optical Flow Based Interpolation of the 4DCT Image Sequences in the External Beam Radiotherapy

Payam Samadi Miyandoab[1,*], Ahmad Esmaili Torshabi[1], Saber Nankali[1]

1- Department of Electrical and Computer Engineering, Kerman Graduate University of Advanced Technology, Kerman, Iran.

Received: 8 March 2015
Accepted: 22 April 2015

ABSTRACT

Purpose- Although in the external beam radiotherapy tumor motionis a crucial and challenging issue due to respiration motion, temporal changes in anatomy during imaging cause considerable problems. Moreover, the Four Dimensional Computed Tomography (4DCT) imaging has been proposed to track these changes at the different breathing phases. Also at real time tumor tracking, the accuracy of motion tracking models that are necessary can be increased by constructing virtual images due to obtaining additional motion data.

Methods- In this study, the 4DCT data set of five real patients who have had lung cancer were provided by DIR-lab site in addition to deformable image registration algorithms presented in MATLAB software and DIRART software respectively to calculate 2D and 3D vector felids between two respiratory volumes. Moreover, the 2D and 3D displacement vector were calculated by optical flow based on Horn-Schunck method, these vector fields were used to generate an interpolated image at the desired time by 2D and 3D interpolation methods. Although 2D interpolation methods included nearest, cubic, linear, and B-spline, the 3D interpolation method was based on the 3D spatial interpolation. In this study, the reconstructed image at the desired time by two methods was compared with real image at the same time. Considering Roots Mean Square Error (RMSE) between actual and interpolated imageis used to measure the accuracy of interpolated images. Also the accuracy of our reconstruction images depends on the accuracy of displacement field.

Results- All of the methods are able to generate images at the desired time with less RMSE and high correlation coefficient. While the 2D interpolation methods that include nearest, cubic, linear, and B-spline were able to generate an image with less errors, the performance of the 2D interpolation method is less efficient than other methods.

Conclusion- The behavior and capability of the algorithmsare demonstrated by synthetic image examples. Furthermore, to compare 2D and 3D optical flow based interpolation methods, the RMSE quantitative measures are calculated. Results indicate that both 2D and 3D interpolation presented methods are outperformed significantly, and the patient is kept away from re-scanning for getting new images.

Keywords:
2D and 3D image reconstruction,
2D and 3D optical flow,
4DCT deformable image registration,
IGRT,
DIRART.

1. Introduction

In the modern radiotherapy, the study of organ motion was significant in the external beam radiotherapy, but to acquire temporal image sequences, modern tomographic imaging devices were enabled [1, 2]. Tumor located in the thorax, abdomen and liver region move due to patient respiration. Due to the respiratory motion, the accuracy of the dose delivery on the tumors and surrounding tissue may not be according to the principle of the ALARA that maybe over and/or under

**** Corresponding Author:***
Payam Samadi Miyandoab, PhD
Department of Electrical and Computer Engineering, Medical Radiation Group, Graduate University of Advanced Technology, Haft Bagh Highway, Knowledge, Paradise, Kerman, Iran.
Tel: (+98) 9366440159 / Fax: (+98) 3412910550
E-mail: p.samadi1989@gmail.com

dosage received by tumors and surrounding tissue [3-6]. Although in the external beam radiotherapy many techniques such as gated radiotherapy [7] and real time tumor tracking [8] are used to reduce the effect of respiratory motion on the accuracy of the dose delivery, the problems of dose delivered at the tumors and surrounding tissue are not yet satisfactorily solved.To overcome tumor motion caused by respiration, the Four-Dimensional (4D) treatment planning dose delivery has been proposed [4]. For the 4D treatment planning and modelling organ motion during the respiratory cycle, the 4DCT data sets have been required [5]. However, the acquisition of the 4DCT data sets which have included time, spatial resolution, and temporal resolution of imaging devices are limited [1, 2, 5]. Moreover, temporal resolution refers to the precision of a measurement with respect to time. Often there is a trade-off between temporal resolution of a measurement and its spatial resolution. In some contexts such as particle physics, this trade-off can be attributed to the finite speed of light and the fact that it takes a certain period of time for the photons carrying information to reach the observer [9]. On this occasion, the system might have undergone changes itself. Thus, the longer the light has to travel; the lower is the temporal resolution.

In the previous study of image processing tasks, image registration algorithms can be classified into intensity (dense) based and feature based. Intensity-based methods compare intensity patterns in images via correlation metrics, while feature-based methods find a correspondence between image features such as points, lines, and contours. Intensity-based methods register entire images or sub-images. If sub-images are registered, centers of corresponding sub images are treated as corresponding feature points [10, 11]. Feature-based methods establish a correspondence between numbers of especially distinct points in images. Knowing the correspondence between a number of points in images, a geometrical transformation is then determined to map the target image to the reference images, thereby establishing point-by-point correspondence between the reference and target images [10, 11]. A spatial and temporal interpolation of data sets is used to calculate the intensity (dense) motion models [12]. However, in processing sequences of images there is great anxiety and a basic problem that the calculated computation of optical flow velocities of the surface points onto the imaging plane of a visual sensor (a type of Opto electronic system to monitoring displacement) an approximation image motion. In particular, optical flow is often a convenient and useful method, but in general there are other motion descriptor methods sometimes more than optical flow [13]. To generate images at predefined phases, a temporal interpolation of the image data is necessary. Moreover, in medical image processing, interpolation is commonly used and is required. In conventional medical image processing, there are numerous techniques for the interpolation of images such as: Grevera and Udupa [14] who divide spatial interpolation methods into two groups: intensity based methods and shape based methods. While See Lehmann *et al*. [15] and Meijeriing [16] tried to compare different intensity based methods, Grevera and Udupa [14] tried to compare the intensity and shape based interpolation methods. On the other hand, for 3D spatial interpolation, other registered interpolation methods based on image volumes were already presented [17, 18]. Goshtasby *et al*. [17] presented a registration based method to interpolate between neighboring slices in tomographic images. While the slices were registered to calculate the intensity values of the interpolated slice from the resulting displacement field by using intensity and gradient features, to identify corresponding points in two adjacent original slices, interpolation lines were calculated. However, to calculate correspondences between neighboring slices Penney *et al*. [18] applied voxel–based registration by using B–spline regularization and the normalized mutual information similarity measure. The interpolation step is a similar method used by Goshtasby [17]. While in particular to consecutive slices, both of the methods were limited, and to the registration algorithm, no theoretical motivations were used. Moreover, the use of the mutual information similarity measure was not motivated by Penney, the concept of interpolation lines were given [18].

Although in this study to interpolate between frames of a temporal image sequence, we used 4DCT sequences images of different patients, the two types of interpolation based on 2D and 3D spatial interpolation were used. Although the 2D interpolation methods included linear, cubic, spline and nearest methods were used, the 3D interpolation was based on 3D spatial interpolation. In addition to calculating 2D and 3D velocity and vector fields at definite time between frames of a temporal image sequence, the Horn-Schunck method basic MATLAB software and the DIRART software respectively were used. To considerate the accuracy of implemented interpolation methods,

the Horn and Schunck's gradient-based algorithm was chosen. In this study, to determine velocity and vector; fields, the first optical flow between the temporal images is determined, and then, velocity is calculated and vector field is used to generate an interpolated image at the desired time. Finally, the results of the two methods of the interpolation are compared with real images at the desired time. Moreover, all of the methods are able to generate images at a predefined phase with less RMSE and high correlation coefficient. While 2D interpolation methods that included nearest, cubic, linear, and B-spline were able to generate images with less errors, the performance of the 2D interpolation method is less efficient than other methods.

2. Material and Methods

2.1. The Properties of the Software and Data

DIRART, deformable image registration (DIR) plus adaptive radiotherapy (ART) research is a large set of programs developed using MATLAB that has implemented in IGRT technology and has potential possibilities for adapting treatment planning on a daily basis. DIRART is designed in a data oriented style with a focus on ability, user-friendliness, performance, accuracy, flexibility, features, configurability and stability. It has a great potential for the ART and DIR research [19-22]. It contains DIR algorithms, common ART functions, integrated graphics, visualization features, and dose metrics analysis functions [19, 23]. In addition to offer more functions, it complementarily works together with CERR (Computational Environment for Radiotherapy Research) [24]. Also DIRART is designed around the concepts of the interactive radiotherapy objects, including images, structures, doses and deformation vector fields (DVF) etc. On the other hand, DIRART provides a full featured working environment for ART related research tasks. It can also rescale, subtract, sum up the transformed doses, and convert iso-dose lines to structures [19, 23 , 25 , and 26]. In this study, the DIRART software was used to calculate 3D velocity and vector field between frames of a temporal image sequence [19, 23 , and 27].

MATLAB is a high-performance language for technical computing [28]. In the MATLAB software, an image registration technique is used widely in medical contexts [29, 30]. Moreover, image registration technique includes a variety of methods such as: interpolation technique, clustering technique, optical flow, segmentation etc. [29, 31]. In this study, 2D and 3D optical flow methods based on Horn-Schunck and 2D and 3D interpolation methods based on the MATLAB software and DIRART software [32, 33] respectively were used to calculate 2D and 3D velocity and vector field between frames of a temporal image sequence and generate 2D and 3D an interpolated images at the desired time [34].

In this study, the data sets used included the 4DCT, of the five patients who have had lung cancer, from the University of Texas Medical Branch, the University of Texas M. D. Anderson Cancer Center, the Office of the Director of the National Institutes of Health through an NIH Director's New Innovator Award, and through an NIH Research Scientist Development Award. Moreover, more information about the patients are shown in Table 1.

Table 1. Shows the Information of the 4DCT Data of Patients.

Number	label	Image dims	Voxels dimensions (mm^3)
Patient 1	4DCT	512×512×128	0.97×0.97×2.5
Patient 2	4DCT	512×512×136	0.97×0.97×2.5
Patient 3	4DCT	512×512×128	0.97×0.97×2.5
Patient 4	4DCT	512×512×128	0.97×0.97 ×2.5
Patient 5	4DCT	512×512×120	0.97 ×0.97×2.5

2.2. The 2D/3D Optical Flow Methods

The initial hypothesis of 2D optical flow based method is that pixel intensities of time varying image regions remain constant. Moreover, the conservation of the intensity of points under motion is formulated in the expression that the total derivative of the image function is zero [30-32]. To calculate vector fields in two images, one must solve the equation (1) of the optical flow constraint equation:

$$I_x u + I_y v + I_t = 0 \quad (1)$$

In the optical flow equation u and v is 2D vector fields. Although to solve the optical flow equation numerous techniques such as Horn-Schuck and Lucas-Kanade Method is used, in this study the Horn-Schuck method is used to calculate velocity

and vector fields [32, 33]. In order to compute a velocity and vector fields matching a pair of consecutive images from a gray value sequence. The consistency of gray level intensity when moving along the flow was computed from the equation (2) of the derivatives in time and space:

$$= \iint \left(I_x u + I_y v + I_t\right)^2 dxdy + \alpha \iint \left\{\left(\frac{\partial u}{\partial x}\right)^2 + \left(\frac{\partial u}{\partial y}\right)^2 + \left(\frac{\partial v}{\partial x}\right)^2 + \left(\frac{\partial v}{\partial y}\right)^2\right\} dxdy \quad (2)$$

In this equation, $\frac{\partial u}{\partial x}$ and $\frac{\partial u}{\partial y}$ are the spatial derivatives of the optical velocity component, and α scales the global smoothness term. Moreover, for each pixel in the image, the Horn-Schunck method minimizes is used in the previous equation to obtain the velocity field, [u v], which is given by the following (3) equation:

$$U_{x,y}^{k+1} = U_{x,y}^{-k} - \frac{I_x[I_x U_{x,y}^{-k} + I_y V_{x,y}^{-k} + I_t]}{\alpha^2 + I_x{}^2 + I_y^2}, \quad (3)$$

$$V_{x,y}^{k+1} = V_{x,y}^{-k} - \frac{I_y[I_x U_{x,y}^{-k} + I_y V_{x,y}^{-k} + I_t]}{\alpha^2 + I_x{}^2 + I_y^2}$$

In this equation $[U_{x,y}^k, V_{x,y}^k]$, is the velocity estimate for the pixel at (x, y), and $[U_{x,y}^{-k}, V_{x,y}^{-k}]$ is the neighborhood average of $[U_{x,y}^k, V_{x,y}^k]$. For k=0, the initial velocity is 0.

To calculate the three-dimensional velocity and vector in the case, the optical flow constraint equation are extending [13]. With considering sequence of 3D images with an intensity value in the volumetric image point (x, y, z) at time t is I (x, y, z, t) that represent intensity values [35, 36]. Moreover, the intensity values are supposed to be described by a differentiable function $I : \Omega \times [0, T] \rightarrow \Re$, the $\Omega \subset \Re^3$ is the imaging volume and T is a strictly positive scalar describing the final time. The partial derivatives of I in the direction of x, y, z and t are denoted by I_x, I_y, I_z and I_t, respectively. Furthermore, the underlying optical flow assumes that image objects keep the same intensity value under motion for at least a short period of time [36-38]. In terms of equations, this can be stated as a flowing question (4):

$$I(x, y, z, t) = I(x + dx, y + dy, z + dz, t + dt) \quad (4)$$

The $(u, v, w) = (\frac{dx}{dt}, \frac{dy}{dt}, \frac{dz}{dt})$ is the 3D velocity vector. For solving this equation denes an ill-posed problem regularization is proposed [38]. To smooth variations in the sense neighboring points, the optical flow is supposed to have almost the same velocity. The Optic Flow Constraint Equation (OFCE) is hence replaced by the equation (5) minimization problem:

$$\min_{(u;v;w)} \int_x \int_y \int_z [(I_x u + I_y v + I_w z + I_t)^2] + \alpha(|\nabla u|^2 + |\nabla v|^2 + |\nabla \omega|^2)] dx\, dy\, dz \quad (5)$$

Moreover, for adjusting the smoothness constraint between the data and the additional α is a positive parameter, and in general to find the best value, it would be required to interactively adjust α.

To solve the equation (5) in the image registration technique, when displacements between the reference and template images are expected to be very large, considering this circumstance the data term to be the squared the difference of the two images without using the 1st order Taylor expansion. The corresponding minimization problem will be then as question (6):

$$\min_{(u;v;w)} \int_x \int_y \int_z [I(x, y, z, t) - I(x+u, y+v, w+z, t+1)^2) + \alpha(|\nabla u|^2 + |\nabla v|^2 + |\nabla \omega|^2)] dx\, dy\, dz \quad (6)$$

Euler-Lagrange equations derived from the minimization problem (5) define a system of three elliptic PDEs with non-constant coefficients depending on the volumetric image data for the zero-order terms. Iterative Gauss Seidel equations

that minimize the Euler-Lagrange equations based on this integral are:

$$\alpha\Delta u - I_x(I_x u + I_y v + I_w z + I_t)=0$$
$$\alpha\Delta v - I_x(I_x u + I_y v + I_w z + I_t)=0$$
$$\alpha\Delta w - I_x(I_x u + I_y v + I_w z + I_t)=0$$

This system is symmetric with respect to the three components of the velocity u, v and w. Thus, a standard way to solve it is the block Gauss-Seidel relaxation as a question (7):

$$u^{k+1} = \bar{u}^{k} - I_x \frac{I_x \bar{u}^{k} + I_y \bar{v}^{k} + I_z \bar{w}^{k} + I_t}{\alpha^2 + I_x^{\,2} + I_y^{\,2} + I_z^{\,2}}$$
$$v^{k+1} = \bar{v}^{k} - I_y \frac{I_x \bar{u}^{k} + I_y \bar{v}^{k} + I_z \bar{w}^{k} + I_t}{\alpha^2 + I_x^{\,2} + I_y^{\,2} + I_z^{\,2}} \qquad (7)$$
$$w^{k+1} = \bar{w}^{k} - I_z \frac{I_x \bar{u}^{k} + I_y \bar{v}^{k} + I_z \bar{w}^{k} + I_t}{\alpha^2 + I_x^{\,2} + I_y^{\,2} + I_z^{\,2}}$$

Where $\bar{u}(resp.\bar{v},\bar{w})$ denotes an average of the neighboring points to $u(resp.v,w)$. This relaxation scheme is known to have slow convergence if the discussion term dominates. We propose then to use a multi grid method to speed up the convergence [35-38]. The u^k, v^k, w^k are 5 × 5 × 5 averages of neighborhoods of velocities at iteration k. We perform a fixed number of iterations as specified by the user (the default is 50 but we usually used 100 or 200).

2.3. The 2D-3D Interpolation Methods

In this study, while the 2D interpolation method included cubic, spline, nearest, and B-spline, the 3D interpolation method was used based on 3D spatial interpolation. 3D spatial interpolation (Non-adaptive interpolation techniques) and 2D interpolation techniques are based on direct manipulation on pixels instead of considering any feature or content of an image [39]. Moreover, for all pixels these techniques follow the same pattern, easy to perform, and have less calculation cost [40].

Nearest interpolation: While this is the simplest and requires the least processing time of all the interpolation algorithms, the nearest neighbor or nearest selects the value of the nearest pixel by rounding the coordinates of the desired interpolation point. Besides, using this method one finds the closest corresponding pixel in the source (original) image for each pixel in the destination image [41]. In addition, new pixels are made the same as others, the pixels or dots of color are duplicated to create new pixels as the image grows. It creates edges that break up curves into steps or jagged edges. This form of interpolation suffers from normally unacceptable effects for both enlargement and reduction of images [42].

Linear Interpolation: To calculate its final interpolated value linear, interpolation takes a weighted average of the 4 neighborhood pixels. Furthermore, the result is a much smoother image than the original image, when all known pixel distances are equal; the interpolated value is simply divided by four. This technique performs interpolation in both directions, horizontal and vertical [40].

Cubic Interpolation: Cubic goes one step beyond linear by considering the closest 4*4 neighborhood of known pixels for a total of 16 pixels. Since these are at various distances from the unknown pixel, closer pixels are given a higher weighting in the calculation. Moreover, perhaps cubic produces noticeably sharper images than the previous two methods, the ideal combination of processing time and output quality [40].

B-Spline interpolation: B-spline interpolation algorithm also interpolates from the nearest sixteen source pixels. However, this algorithm uses B-spline interpolating functions instead of cubic splines, which in general yield quite smooth results. Also it performs a convolution with a two-dimensional non separable filter, so its complexity is increased. Despite this performance difference, cubic B-spline has interesting characteristics of smoothness that make it a good option in some cases. In contrast, cubic interpolation uses a convolution with a separable filter, and hence has less complexity [41].

3D spatial interpolation: 3D spatial modeling permits the flexibility to create vertical and horizontal cutting planes. It also provides a better insight to spatial variations than 2D representations. Besides, 3D spatial modeling with geo-statistical methods is appropriate for representation and analyses of pelagic variables, the 3D spatial interpolation method also gives a more comprehensive picture of the phenomena [43-46].

3. Results

To test and evaluate the performance of the methods, the correlation coefficient (R) and Root Mean Square Error (RMSE) were expressed between images at desired time and interpolation image according the (8) following metric equation:

$$RMSE = \sqrt{\frac{1}{N}\sum_{i=1}^{N}(A_i - P_i)^2} \quad (8)$$

where, N is the number of samples, A_i is the i_{th} actual image in the dataset, and P_i is the i_{th} interpolation image.

To generate images at predefined phases, the five frames of each patient were considered to evaluate the performance and compare results of the 2D and 3D interpolation methods. Moreover, the 2D interpolation methods included four methods (nearest, linear, spline, and cubic), the 3D interpolation method was based on 3D spatial interpolation. To calculate 2D and 3D velocity and vector fields, the optical flow method based on the Horn-Schuck was available, and to evaluate the performance of each method the correlation coefficient and RMSE was considered. Also more information about the amount of the RMSE and correlation coefficient is shown in the Table 2.

The results of interpolation, frames, and RMSE of patient images are shown in Figure 1. Furthermore, the results of the interpolation images which are shown in Figure 1 respectively are Cubic, Spline, Linear, Nearest, and Spatial, real images interpolation images and RMSE between two images are shown in each column. In addition, these images were considered in the middle frame of the 4DCT sequence images.

Table 2. The RMSE and correlation coefficient for each 2D and 3D interpolation methods were calculated.

		Methods				
		Optical flow (script MATLAB)			DIRART software	
Patient	Phase	correlation		RMSE (mm)	correlation	RMSE (mm)
Patient one	T50 and T70	nearest	0.99227	5.5391	0.9906	6.0738
		linear	0.99245	5.4655		
		Spline	0.99208	5.6175		
		cubic	0.99204	5.5712		
Patient two	T50 and T70	nearest	0.99551	4.3192	0.9953	4.4140
		linear	0.99553	4.3216		
		Spline	0.99533	4.4057		
		cubic	0.99533	4.3762		
Patient three	T50 and T70	nearest	0.99465	4.15702	0.9239	15.6184
		linear	0.99520	3.93037		
		Spline	0.99496	4.03525		
		cubic	0.99493	4.01136		
Patient four	T50 and T70	nearest	0.99802	2.90117	0.9990	2.1784
		linear	0.99789	2.99991		
		Spline	0.99778	3.06389		
		cubic	0.99778	3.03238		
Patient five	T50 and T70	nearest	0.98935	6.1338	0.9890	6.4027
		linear	0.98906	6.21801		
		Spline	0.98876	6.29249		
		cubic	0.98876	6.26684		

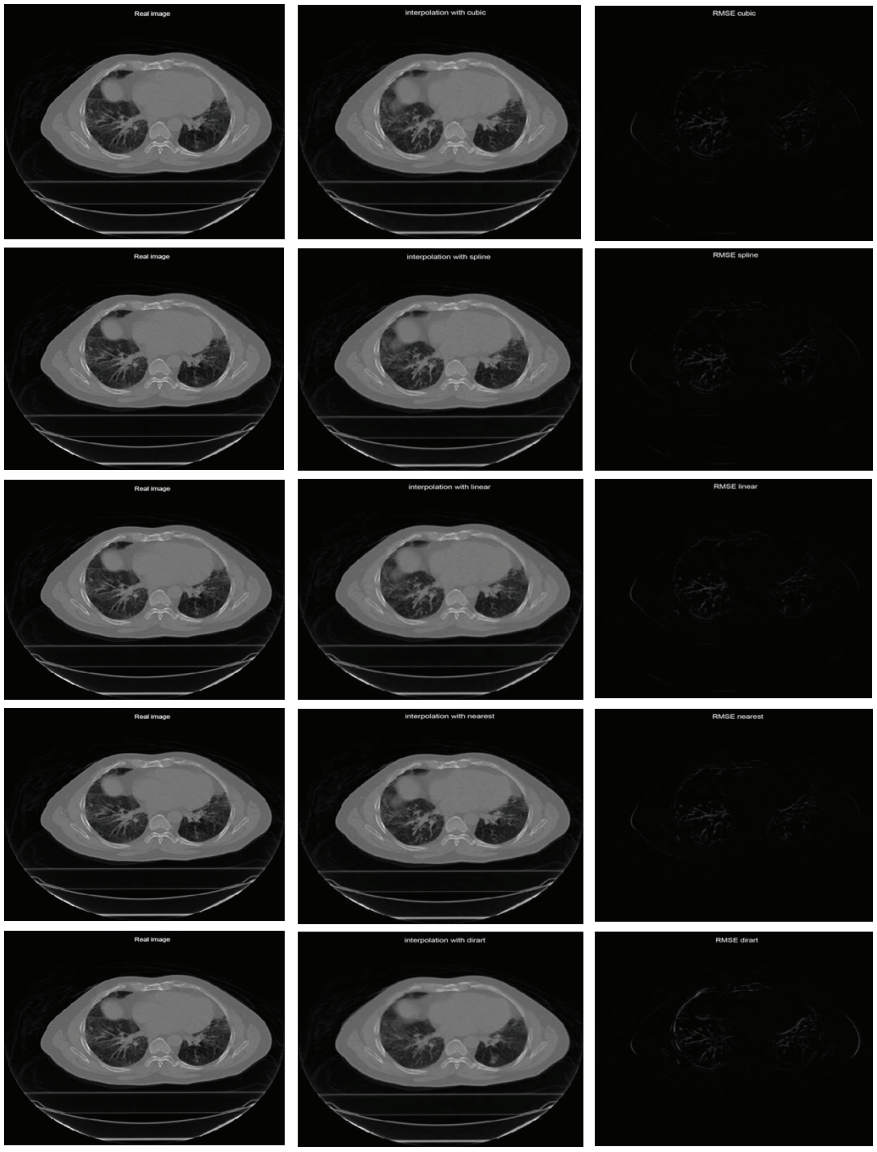

Figure 1. Shows the frames of patient images, the results of interpolation of the middle image, and RMS that considered between two sequence images.

4. Discussion

Although in the image registration technique many methods and strategies have been appeared to estimate image motion, image motion remains a challenging task and no techniques are able to generate accuracy sufficiently. To recover the motion and scene parameters in a realistic environment, the optical flow vector fields are proposed. In fact, to carry useful 3D and 2D motion and structure computations, motion and structure algorithms with high accuracy and less error are needed. In this study, a method has been available to computing optical flow from a sequence of images. The optical flow is based on the Horn-Schuck with the smoothness of the flow. To calculate the velocity and vector fields an iterative method was considered. After calculating velocity and vector fields, the interpolating temporal image sequences were represented. Moreover, the interpolation algorithm was theoretically derived from the optical flow equation; the performance of the algorithm was evaluated qualitatively and quantitatively. The quantitative results show that the optical flow based method clearly outperforms the linear and shape based interpolation. The presented method is also applicable to interpolate between neighboring slices in spatial tomographic images. An evaluation of this approach is accomplished at present.

To calculate 2D and 3D velocity and vector fields, the MATLAB and DIRART software were used respectively. The 2D and 3D velocity and vector fields based on the 2D and 3D interpolation methods were used to generate an image at the desired time. In this study although 2D interpolation method included linear, spline, nearest, cubic was used, 3D interpolation was based on 3D spatial interpolation. Moreover, results of the interpolation are shown in the Figure 1 and Table 2. As seen in the Table 2, all of the methods were able to generated images at a predefined phase with less RMSE and high correlation coefficient. Also the 2D interpolation methods were able to generate an image with less error than the 3D interpolation method. Thus, if the velocity and vector field is known, we can interpolate the image at the predefined frame. But in general the intensity conservation assumption might not be fulfilled and structures may appear or disappear between two time steps. Therefore, we use a weighted average between corresponding voxels in the adjacent timeframes.

Furthermore, in our experiments the 2D and 3D interpolation methods were computationally less expensive than the shape based interpolation. The performance of the shape based method strongly depends on the implementation of the distance transformation. In this study we used the algorithm of Danielsson [47], but faster algorithms exist [48]. Although in contrast performance of the optical flow based interpolation, the shape based method is independent of the dynamic range of the images, the Goshtasby *et al*. [17] and Penney *et al*. [18] algorithm shows a symmetric behavior. As a drawback of our method, the Gaussian regularization is not guaranteed and the inverse applies to all points.

A deformable image registration matrix, describing the deformation of a 4DCT image data set from one phase of the respiratory cycle to the other, obtained by the use of an optical flow algorithm can be used to generate 4DCT image data set at the desired time that provided a set of contours of normal anatomic structures and the GTV in all phases of a 4DCT image data set. Therefore, further research will address the integration of other regularization techniques and other techniques. Moreover, to generate 4DCT image data set at the desired time, an evaluation performance of different strategies of the optical flow, and interpolation method to calculate the velocity and victors' field is needed.

Acknowledgment

The authors acknowledge Dr. Richard Castillo Assistant Professor University of the Texas Medical Branch, the University of the Texas M. D. Anderson Cancer Center, and the Office of the Director of the National Institutes of Health through an NIH Director's New Innovator Award (DP2OD007044), and through an NIH Research Scientist Development Award (1K01CA181292-01) for providing access to the 4DCT datasets.

Reference

1- A. F. Frangi, W. J. Niessen, and M. A. Viergever, "Three-dimensional modeling for functional analysis of cardiac images, a review," *Medical Imaging, IEEE Transactions on,* vol. 20, pp. 2-5, 2001.

2- D. A. Low, M. Nystrom, E. Kalinin, P. Parikh, J. F. Dempsey, J. D. Bradley, S. Mutic, S. H. Wahab, T. Islam, and G. Christensen, "A method for the reconstruction of four-dimensional synchronized CT scans acquired during free breathing," *Medical physics,* vol. 30, pp. 1254-1263, 2003.

3- A. Torshabi, A. Pella, M. Riboldi, and G. Baroni, "Targeting accuracy in real-time tumor tracking via external surrogates: a comparative study," *Technology in cancer research & treatment,* Vol. 9, pp. 551-561, 2010.

4- P. Keall, V. Kini, S. Vedam, and R. Mohan, "Motion adaptive x-ray therapy: a feasibility study," *Physics in medicine and biology,* vol. 46, p. 1, 2001.

5- P. Keall, "4-dimensional computed tomography imaging and treatment planning," in *Seminars in radiation oncology*, pp. 81-90, 2004.

6- S. Webb, "IMRT delivery techniques," in *Image-guided imrt*, ed: Springer, pp. 73-90, 2006.

7- H. D. Kubo and B. C. Hill, "Respiration gated radiotherapy treatment: a technical study," *Physics in medicine and biology,* vol. 41, p. 83, 1996.

8- A. E. Torshabi, M. Riboldi, A. A. I. Fooladi, S. M. M. Mosalla, and G. Baroni, "An adaptive fuzzy prediction model for real time tumor tracking in radiotherapy via external surrogates," *Journal of Applied Clinical Medical Physics,* vol. 14, 2013.

9- R. J. Walledge, R. Manavaki, M. Honer, and A. J. Reader, "Inter-frame filtering for list-mode EM reconstruction in high-resolution 4-D PET," *Nuclear Science, IEEE Transactions on,* vol. 51, pp. 705-711, 2004.

10- A. Behan, "2-D and 3-D Image Registration For Medical,

Remote Sensing, and Industrial Applications," *The Photogrammetric Record,* vol. 21, pp. 180-181, 2006.

11- A. A. Goshtasby, *2-D and 3-D image registration: for medical, remote sensing, and industrial applications*: John Wiley & Sons, 2005.

12- W. Enkelmann, "Investigations of multigrid algorithms for the estimation of optical ow elds in image sequences," Comp. Vision, Graphics, and Im," *in Proc*, p. 150177, 1988.

13- R. Battiti, E. Amaldi, and C. Koch, "Computing optical flow across multiple scales: an adaptive coarse-to-fine strategy," *International journal of computer vision,* vol. 6, pp. 133-145, 1991.

14- G. J. Grevera and J. K. Udupa, "An objective comparison of 3-D image interpolation methods," *Medical Imaging, IEEE Transactions on,* vol. 17, pp. 642-652, 1998.

15- T. M. Lehmann, C. Gonner, and K. Spitzer, "Survey: Interpolation methods in medical image processing," *Medical Imaging, IEEE Transactions on,* Vol. 18, pp. 1049-1075, 1999.

16- J. Ehrhardt, D. Säring, and H. Handels, "Optical flow based interpolation of temporal image sequences," *in Proc. of SPIE* , pp. 61442K-1 , 2006.

17- A. Goshtasby, D. A. Turner, and L. V. Ackerman, "Matching of tomographic slices for interpolation," *Medical Imaging, IEEE Transactions on,* vol. 11, pp. 507-516, 1992.

18- G. P. Penney, J. A. Schnabel, D. Rueckert, M. A. Viergever, and W. J. Niessen, "Registration-based interpolation," *Medical Imaging, IEEE Transactions on,* vol. 23, pp. 922-926, 2004.

19- D. Yang, I. El Naqa, A. Aditya, Y. Wu, M. Goddu, S. Mutic, J. O. Deasy, and D. A. Low, "DIRART–A Software Suite for Deformable Image Registration and Adaptive Radiotherapy Research," in *World Congress on Medical Physics and Biomedical Engineering, September 7-12, 2009, Munich, Germany*, pp. 844-847 , 2009.

20- C. Tyson, C. McAndrew, P. Tuma, I. Pegg, and A. Sarkar, "Automated nonparametric method for detection of step-like features in biological data sets," *Cytometry Part A,* 2015.

21- R. L. Smith, D. Yang, A. Lee, M. L. Mayse, D. A. Low, and P. J. Parikh, "The correlation of tissue motion within the lung: implications on fiducial based treatments," *Medical physics,* vol. 38, pp. 5992-5997, 2011.

22- C. Knill, T. Bossenberger, J. Rakowski, E. Wennerstrom, and M. Snyder, "Deformable Image Registration (DIRART) Testing Using Thin-Plate Spline Deformations," *International Journal of Radiation Oncology' Biology' Physics,* Vol. 81, p. S820, 2011.

23- D. Yang, S. R. Chaudhari, S. M. Goddu, D. Pratt, D. Khullar, J. O. Deasy, and I. El Naqa, "Deformable registration of abdominal kilovoltage treatment planning CT and tomotherapy daily megavoltage CT for treatment adaptation," *Medical physics,* vol. 36, pp. 329-338, 2009.

24- J. O. Deasy, A. I. Blanco, and V. H. Clark, "CERR: a computational environment for radiotherapy research," *Medical physics,*vol. 30, pp. 979-985, 2003.

25- J.-P. Thirion, "Image matching as a diffusion process: an analogy with Maxwell's demons," *Medical image analysis,* Vol. 2, pp. 243-260, 1998.

26- D. Yang, H. Li, D. A. Low, J. O. Deasy, and I. El Naqa, "A fast inverse consistent deformable image registration method based on symmetric optical flow computation," *Physics in medicine and biology,* Vol. 53, p. 6143, 2008.

27- J. L. Barron, D. J. Fleet, and S. S. Beauchemin, "Performance of optical flow techniques," *International journal of computer vision,* Vol. 12, pp. 43-77, 1994.

28- M. Grant, S. Boyd, and Y. Ye, "CVX: Matlab software for disciplined convex programming," ed, 2008.

29- S. L. Keeling and W. Ring, "Medical image registration and interpolation by optical flow with maximal rigidity," *Journal of Mathematical Imaging and Vision,* vol. 23, pp. 47-65, 2005.

30- R. C. Gonzalez, R. E. Woods, and S. L. Eddins, *Digital image processing using MATLAB*: Pearson Education India, 2004.

31- M. Lefébure and L. D. Cohen, "Image registration, optical flow and local rigidity," *Journal of Mathematical Imaging and Vision,* vol. 14, pp. 131-147, 2001.

32- A. Bruhn, J. Weickert, and C. Schnörr, "Lucas/Kanade meets Horn/Schunck: Combining local and global optic flow methods," *International journal of computer vision,* vol. 61, pp. 211-231, 2005.

33- based on a theory for warping," in *Computer Vision-ECCV 2004*, ed: Springer, pp. 25-36 , 2004.

34- J. Modersitzki, *FAIR: flexible algorithms for image registration* Vol. 6: SIAM, 2009.

35- G. J. Klein and R. H. Huesman, "A 3D optical flow approach to addition of deformable PET volumes," in *Nonrigid and Articulated Motion Workshop, 1997. Proceedings., IEEE*, pp. 136-143 , 1997.

36- J. Barron and N. Thacker, "Tutorial: Computing 2D and 3D optical flow," *Imaging Science and Biomedical Engineering Division, Medical School, University of Manchester,* 2005.

37- S. M. Song and R. M. Leahy, "Computation of 3-D velocity fields from 3-D cine CT images of a human heart," *Medical Imaging, IEEE Transactions on,* vol. 10, pp. 295-306, 1991.

38- E. M. Kalmoun, H. Köstler, and U. Rüde, "Parallel multigrid computation of the 3D optical flow," Technical Report 04-4, Friedrich-Alexander-Universität Erlangen-Nürnberg, Lehrstuhl für Informatik 10 (Systemsimulation) 2004.

39- W. Burger and M. J. Burge, *Digital image processing: an algorithmic introduction using Java*: Springer Science & Business Media, 2009.

40- enhancement," *Journal of Emerging Technology and Advanced Engineering,* vol. 3, 2013.

41- P. Miklos, "Image interpolation techniques," in *2nd Siberian-Hungarian Joint Symposium On Intelligent Systems*, 2004.

42- P. Chennarao, V. Vishnupriya, K. Anjali, P. Jayasree, and P. Pridhvi, "A Novel Method for Satellite Image Contrast Enhancement Using Interpolation."

43- J. Sahlin, M. A. Mostafavi, A. Forest, and M. Babin, "Assessment of 3D Spatial Interpolation Methods for Study of the Marine Pelagic Environment," *Marine Geodesy,* vol. 37, pp. 238-266, 2014.

44- O. Falivene, L. Cabrera, and A. Sáez, "Optimum and robust 3D facies interpolation strategies in a heterogeneous coal zone (Tertiary As Pontes basin, NW Spain)," *International Journal of Coal Geology,* vol. 71, pp. 185-208, 2007.

45- Z.-h. Lin, X.-g. MO, H.-x. LI, and H.-b. LI, "Comparison of Three Spatial Interpolation Methods for Climate Variables in China [J]," *Acta Geographica Sinica,* Vol. 1, p. 005, 2002.

46- W.-C. Lin, C.-C. Liang, and C.-T. Chen, "Dynamic elastic interpolation for 3D medical image reconstruction from serial cross sections," *Medical Imaging, IEEE Transactions on,* vol. 7, pp. 225-232, 1988.

47- P.-E. Danielsson, "Euclidean distance mapping," *Computer Graphics and image processing,* vol. 14, pp. 227-248, 1980.

48- C. R. Maurer Jr, R. Qi, and V. Raghavan, "A linear time algorithm for computing exact Euclidean distance transforms of binary images in arbitrary dimensions," *Pattern Analysis and Machine Intelligence, IEEE Transactions on,* Vol. 25, pp. 265-270, 2003.